

## Integrity Capability of Standalone GPS

***Elizabeth Smith***

UNSW/DST Group/Australia  
(08) 7389 6438 [liz.smith@dst.defence.gov.au](mailto:liz.smith@dst.defence.gov.au)

***Mark Knight***

DST Group/Australia  
(08) 7389 6864 [mark.knight@dst.defence.gov.au](mailto:mark.knight@dst.defence.gov.au)

***Andrew Dempster***

UNSW/Australia  
(02) 9385 6890 [a.dempster@unsw.edu.au](mailto:a.dempster@unsw.edu.au)

***Joon Wayn Cheong***

UNSW/Australia  
(02) 9385 6702 [cjwayn@unsw.edu.au](mailto:cjwayn@unsw.edu.au)

### ABSTRACT

A vehicle was driven around a rural environment in Albert Park, Victoria and an urban environment in Melbourne CBD. The GPS receiver data was collected and processed to determine the position of the vehicle and its associated position errors and Horizontal Protection Levels (HPL). It was found that the HPL calculated for the CBD serials did not accurately reflect the calculated position error of the vehicle, unlike the Albert Park data which showed consistency between predicted and measured errors. The cause of the inconsistencies in the CBD data is postulated to be due to multipath signals contaminating the data, which is supported through simulation. The faulty satellite pseudoranges were removed using a Fault Detection and Exclusion process to improve the calculated and reported errors. The conclusion of this paper is that GPS alone is not capable of providing accurate position error estimations within urban environments and is limited in its integrity monitoring capability due to a lack of visible satellites.

**KEYWORDS:** Cooperative Intelligent Transport Systems(CITS), GPS, Horizontal Protection Level (HPL), Integrity, Receiver Autonomous Integrity Monitoring (RAIM)

## 1. INTRODUCTION

The Global Positioning System (GPS) developed by the United States Department of Defense has provided increasingly better accuracies over time since selective availability was turned off in 2001 (Ochieng & Sauer, 2002). However, GPS is not without its own sources of error, particularly in an urban environment. Multipath and non-line of sight propagation due to tall buildings add up to unreliable and inaccurate positioning for vehicles (Blanch *et al.*, 2013).

This paper demonstrates the integrity capabilities of standalone GPS in an urban environment. The Stanford Integrity Diagram (Tossaint *et al.*, 2007) is used to display the integrity availability of GPS in both open and dense urban areas of Melbourne during a vehicular experiment in 2015. The Protection Level Toolbox in Matlab (D. Bruckner, 2014) is used to calculate the horizontal protection level for a vehicle in open and dense urban environments. This paper will show that GPS alone does not have sufficient integrity capabilities to overcome the error sources in urban environments.

The RAIM and Fault Detection and Exclusion (FDE) algorithms used in this analysis and the Stanford Integrity Diagram used to display the data are outlined in Sections 2 and 3, respectively. Section 4 details the experiment that generated the GPS data and how it was processed, and Section 5 describes the results of the analysis. The conclusions from the results and proposed way forward with cooperative positioning is presented in Section 6. The aim of this paper is to demonstrate the capabilities of RAIM in an urban environment.

## 2. RAIM

Receiver Autonomous Integrity Monitoring (RAIM) has been improved upon and expanded many times in the literature. It was originally designed for GPS only in the aviation space (ICAO, 2001), however it has been adapted to the changing navigation requirements of today. Examples are extended RAIM that includes other sensors, such as Inertial Navigation Systems (INS) (Hewitson & Wang, 2010) and advanced RAIM that takes into account the different positioning constellations (Blanch *et al.*, 2013). Within RAIM there are multiple methods of calculating the range residual error and test statistic. However, (Brown, 1992) showed that all methods are equivalent; just different in complexity.

The RAIM algorithm used for this work is a least squares based snapshot method detailed in the thesis from Ohio University that is behind the Matlab Protection Level Toolbox code (D. C. Bruckner, 2010). The code, downloadable from Mathworks (D. Bruckner, 2014), allows the protection levels to be calculated in six different ways depending on biases and weighting methodology. The Local Area Augmentation System (LAAS) method (method 1) was used to process the data presented in Section 5. This method was chosen as it is a baseline representation of the protection level associated with a fault probability as described in (ICAO, 2001).

The Horizontal Protection Level (HPL) is a measure of the trust in the position solution provided based on the satellite geometry available and the residual errors in position estimation. The HPL is calculated in this methodology through the following sequence of equations (D. C. Bruckner, 2010).

The linearised measurement equation for GPS is given by:

$$y = Hx + \varepsilon$$

Where:

$y$  -  $n \times 1$  vector made up of the difference in pseudorange measurements from expected and measured values

$x$  -  $4 \times 1$  vector containing the offset in  $x$ ,  $y$ ,  $z$ , and time from the true position.

$\varepsilon$  -  $n \times 1$  measurement error vector.

$n$  - number of pseudorange measurements.

$H$  -  $n \times 4$  geometry matrix given in the form:

$$H = \begin{bmatrix} x_1 & y_1 & z_1 & 1 \\ x_2 & y_2 & z_2 & 1 \\ \vdots & \vdots & \vdots & \vdots \\ x_n & y_n & z_n & 1 \end{bmatrix}$$

where  $x$ ,  $y$ ,  $z$  are the unit vectors pointing from receiver to satellite in the ENU reference frame.

The vector  $y$  in the linearised measurement equation is calculated from what is measured and the output from an estimation process such as a Kalman filter. The vector  $x$  is the desired output in the position space. In this paper,  $x$  is estimated using non-weighted least squares calculated using the following equation:

$$\begin{aligned} \hat{x}_{LS} &= (H^T H)^{-1} H^T y \\ &= S y \end{aligned}$$

where:

$$S = (H^T H)^{-1} H^T$$

Using the probability of failure and the  $S$  matrix defined above, the horizontal protection level for an epoch can be calculated using:

$$HPL = K_{ffmd} d_{major}$$

where  $K_{ffmd}$  is a scale factor (see next page), and  $d_{major}$  is the uncertainty error within 1 standard deviation aligned in the direction of the major axis of the error ellipse given by:

$$d_{major} = \sqrt{\frac{d_x^2 + d_y^2}{2} + \sqrt{\left(\frac{d_x^2 - d_y^2}{2}\right)^2 + d_{xy}^2}}$$

where:

$$d_x^2 = \sum_{i=1}^n s_{1,i}^2 \sigma_i^2$$

$$d_y^2 = \sum_{i=1}^n s_{2,i}^2 \sigma_i^2$$

$$d_{xy}^2 = \sum_{i=1}^n s_{1,i} s_{2,i} \sigma_i^2$$

with:

$s_{1,i}$   $s_{2,i}$  - east and north elements of  $S$  matrix

$\sigma_i^2$  - the variance of the  $i^{th}$  satellite pseudorange measurement

$K_{ffmd}$  is a scale factor based on the probability of failure in the system calculated by:

$$K_{ffmd} = -\sqrt{2} \cdot \text{erfcinv} \left( 2 \left( 1 - \frac{(1 - prob)}{2} \right) \right)$$

where:

$\text{erfcinv}$  -the inverse complementary error function

$prob$  – integrity probability of failure

These equations allow the HPL to be calculated as a function of the satellite geometry, the estimated receiver position and satellite errors, and the integrity probability of failure.

## 2.1 Fault detection and exclusion

The main source of error analysed in this process is multipath due to the vehicle travelling in an urban environment. For RAIM to work effectively, the multipath data points need to be accounted for during processing. A method of fault detection and exclusion is detailed in (Jiang *et al.*, 2011) which is the method used here.

The first step in the process is to calculate a test statistic that will allow a condition based approach to fault detection. This is done with first calculating the residual vector ( $w$ ) based on the satellite geometry ( $H$ ) and estimated pseudorange errors ( $y$ ):

$$w = [I - H(H^T H)^{-1} H^T] y$$

$$= y - H \hat{x}_{LS}$$

The residual vector is then used to calculate the Sum of Squares Error (SSE):

$$SSE = w^T w$$

The SSE becomes part of the calculation for the test statistic along with the degrees of freedom ( $dof$ ) given by  $n - 4$  satellites.

$$Test\ Statistic = \sqrt{\frac{SSE}{dof}}$$

where  $dof = n - 4$ , and  $n > 4$  for fault detection capability. Once the test statistic is known, a threshold needs to be calculated; above which a fault is declared. The threshold is

calculated using a normalised chi-squared distribution ( $T_{chi}$ ) based on a given probability (here:  $10^{-7}$ ) and the degrees of freedom.

$$Threshold = \sigma \sqrt{\frac{T_{chi}}{dof}}$$

Where  $\sigma$  is the assumed standard deviation of the measurement error.

When the test statistic is greater than the threshold, an error is detected.

$$Test\ Statistic > Threshold \rightarrow Error\ Detected$$

If an error is detected, the maximum  $y$  value for that epoch is removed as well as the corresponding row in  $H$  (generating a new matrix  $H'$ ). The estimated position error is then calculated using  $H'$  and reduced  $y$  vector,  $y'$ , as follows:

$$\hat{x}'_{LS} = (H'^T H')^{-1} H'^T y'$$

Based on the iterative Newton-Raphson method, the new position estimate,  $x'$ , can be determined by taking the previous position estimate,  $x$ , and the position error estimate,  $\hat{x}'_{LS}$ , into account.

$$x' = x - \hat{x}'_{LS}$$

A new  $H$  matrix is then calculated using the new position estimate and the satellite positions, where the new unit direction vectors for the  $H''$  matrix are given by

$$\frac{(s - x')}{\|s - x'\|}$$

where  $s$  is the satellite position.

$H''$  is then used with  $y'$  to calculate the new position error:

$$\hat{x}'_{LS2} = (H''^T H'')^{-1} H''^T y'$$

$H''$  is used to then calculate the HPL. This is plotted against the altered position error given by  $\hat{x}'_{LS2}$  in the Stanford Integrity Diagram.

### 3. STANFORD INTEGRITY DIAGRAM

The Stanford Integrity Diagram was developed by Stanford University to represent the relationship between protection levels and position errors for Satellite Based Augmentation Systems (SBAS) (Tossaint *et al.*, 2007). Figure 1 shows the generalised layout of the integrity diagram with descriptions of the impact of each section. The plot shows the true position error (PE) along the x axis and the calculated protection level (PL - horizontal or vertical) along the y axis. All data points for every epoch are displayed in a colour scale and binned in PL/PE pairs (colour indicates number of occurrences of the pair). The purpose of the diagram is to understand the integrity of a data set visually and the impacts of the results.

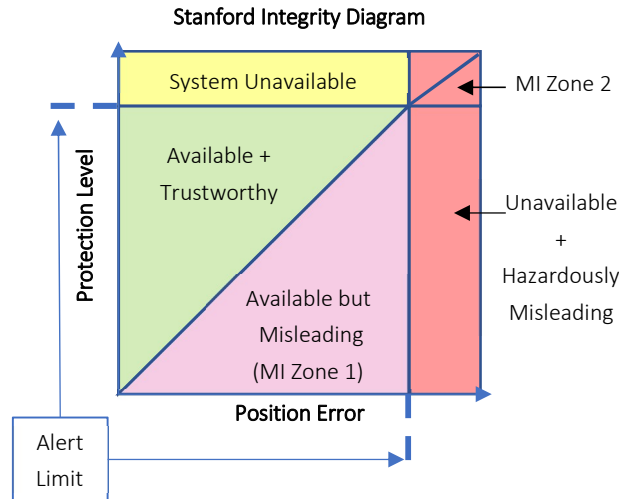


**Figure 1:** Representation of the Stanford Integrity Diagram based on the work in (Tossaint *et al.*, 2007)

The position within the diagram that a PE/PL pair falls into characterises the epoch in terms of availability or misleading information. The quantitative criteria for this with respect to a set Alarm Limit (AL) is given in Table 1.

Condition	Result
$PL < PE < AL$	Available + Trustworthy
$PL < PE > AL$	Unavailable
$PL > PE < AL$	Available + Misleading
$PL > PE > AL$	Unavailable + Hazardously Misleading

**Table 1:** Integrity availability based on the Stanford Integrity Diagram (Tossaint *et al.*, 2007)

The original purpose for the diagram was for quantifying SBAS and Wide Area Augmentation Systems (WAAS) integrity (Hansen, 1997). This inherently involves the use of corrected position information to determine the true position error. To use this in vehicles requires similar post processing to determine the true error. For use in real time applications, a different method will need to be used to determine position error, potentially being the difference between estimated (predicted) position based on say a Kalman Filter and measured position.

#### 4. EXPERIMENT AND DATA COLLECTION

A vehicle was driven around Melbourne, Australia collecting GPS, GLONASS, Inertial Navigation System (INS) and Ultra-Wide Band (UWB) data. One test serial involved the vehicle traversing Albert Park and the other, the Central Business District (CBD). The comparison of the two scenarios will show the difference between GPS integrity in open and urban environments without any Fault Detection and Exclusion (FDE) taking place.

The vehicle's true position was determined by post processing the GPS data in RTKLib (Takasu, 2011) where differential corrections were used to resolve the position to a higher accuracy. Figure 2 shows the truth and measured positions of the vehicle as it travelled around Albert Park (a) and Melbourne CBD (b).

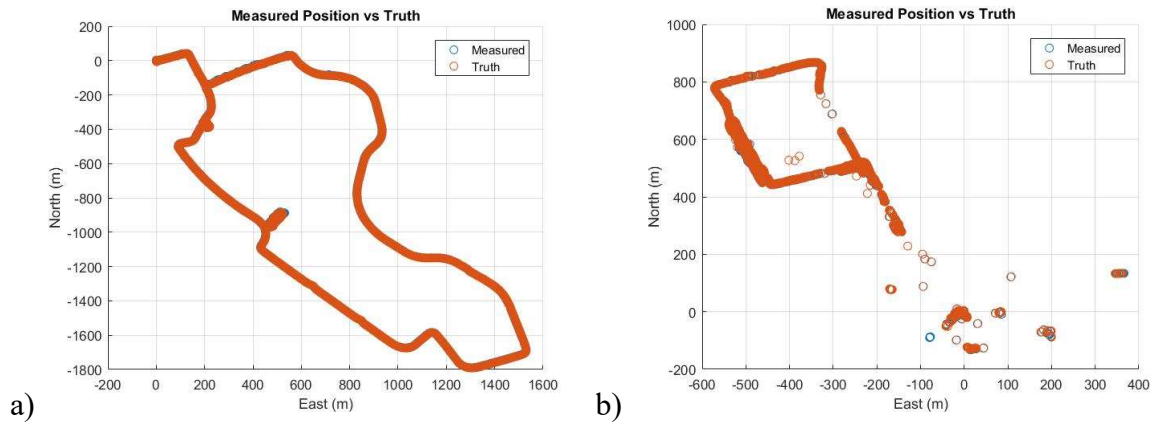


**Figure 2:** The path travelled around Albert Park (a) and through Melbourne CBD (b). The orange circles represent the position after post processing (truth), the blue circles represent the position as measured during the experiment

The test around Albert park took approximately 20 minutes which involved two cars driving in sequence. The CBD test was conducted over a similar time period; however, the vehicles had to leave the city centre to get a position fix before beginning the test which corresponds to the rectangle on the right of Figure 2b.

Both cars were fitted with a Leica GS10 GNSS receiver and antenna. The antenna was positioned on a plate with the INS, UWB and DSRC units. Figure 3 shows the layout on the plate mounted to each vehicle.

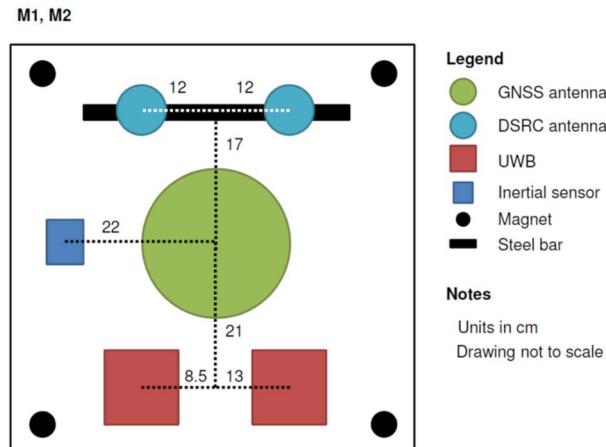


**Figure 3:** Equipment layout on a mounting plate fixed to each vehicle

## 5. RESULTS AND DISCUSSION

The horizontal protection levels (HPL), position errors and FDE results are presented in this section. The open sky test around Albert Park is compared with the urban canyon of Melbourne CBD to observe the effect of multipath on the HPL.

The position error between the original measured position and the post processed accurate position (considered truth) is shown in Figure 4. Notice the difference in scale between the Albert Park test and the CBD test position errors.

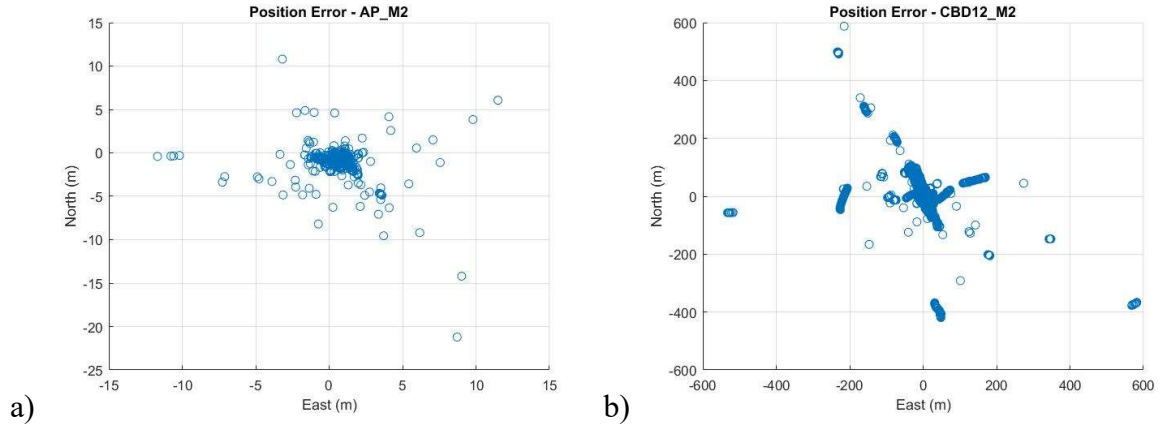


**Figure 4:** The difference in position between measured and truth data for the Albert Park circuit (a) and Melbourne CBD (b)

The high position errors in the CBD test could be due to multipath, lack of visible satellites or a combination of both.

### 5.1 Horizontal Protection Levels

Running the receiver and satellite position data through the Protection Level Toolbox in Matlab calculates the associated HPL for that data set. The HPL are plotted against the corresponding horizontal position errors. The comparison between open air data and urban canyon is shown in Figure 5.

The difference between Albert Park and Melbourne CBD is quite significant. The amount of data points to the right of the diagonal line in Figure 5b shows that RAIM is incapable of dealing with other sources of error; such as multipath; in its current state. The basic algorithm could not predict the position errors that were found during the tests in Melbourne CBD. This is because the algorithm is based on satellite geometry and not line of sight to the satellites.

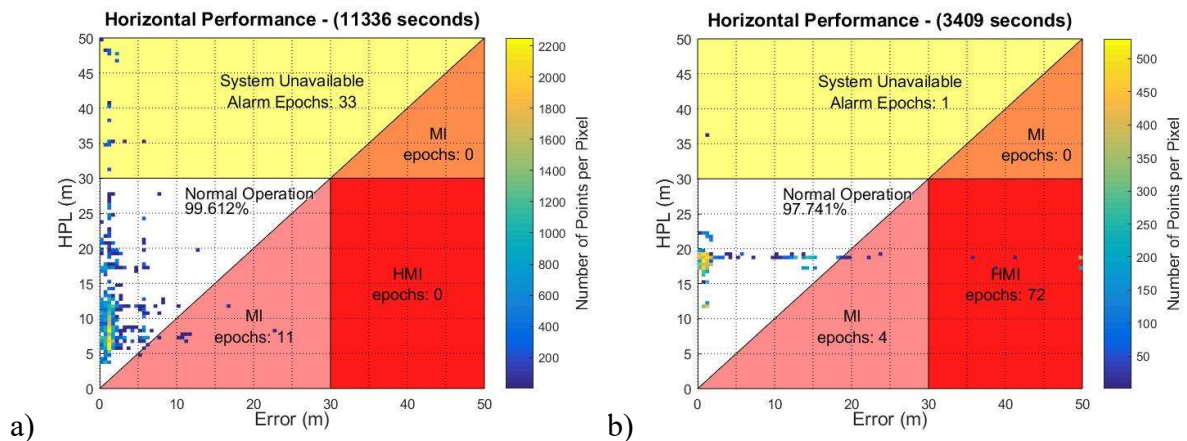


**Figure 5:** Comparison of Integrity Diagrams for Albert Park (a) and Melbourne CBD (b) calculated for a failure rate of  $10^{-7}$  and assuming  $\sigma_i^2 = \sigma^2 = UERE$

The data points shown in Figure 5 show the number of points in each bin, given by a colour, and the total number of points processed displayed in the title of the figure. The significantly



lower data points for the CBD test is an indicator of already too few satellites visible during the test when compared to Albert Park.

## 5.2 Multipath Effects

To test the assumption made earlier that the scatter in the CBD plot was due to multipath, further analysis was conducted on the Albert Park data. The pseudorange for one satellite was increased by 20 m on 50% of the epochs. The satellite selection was random as was the epoch it was applied to. The changed pseudoranges were then used to calculate the position errors and new Stanford Integrity Diagrams were generated. Figure 6a) and b) show the shift of data to the right as the pseudorange error is added.

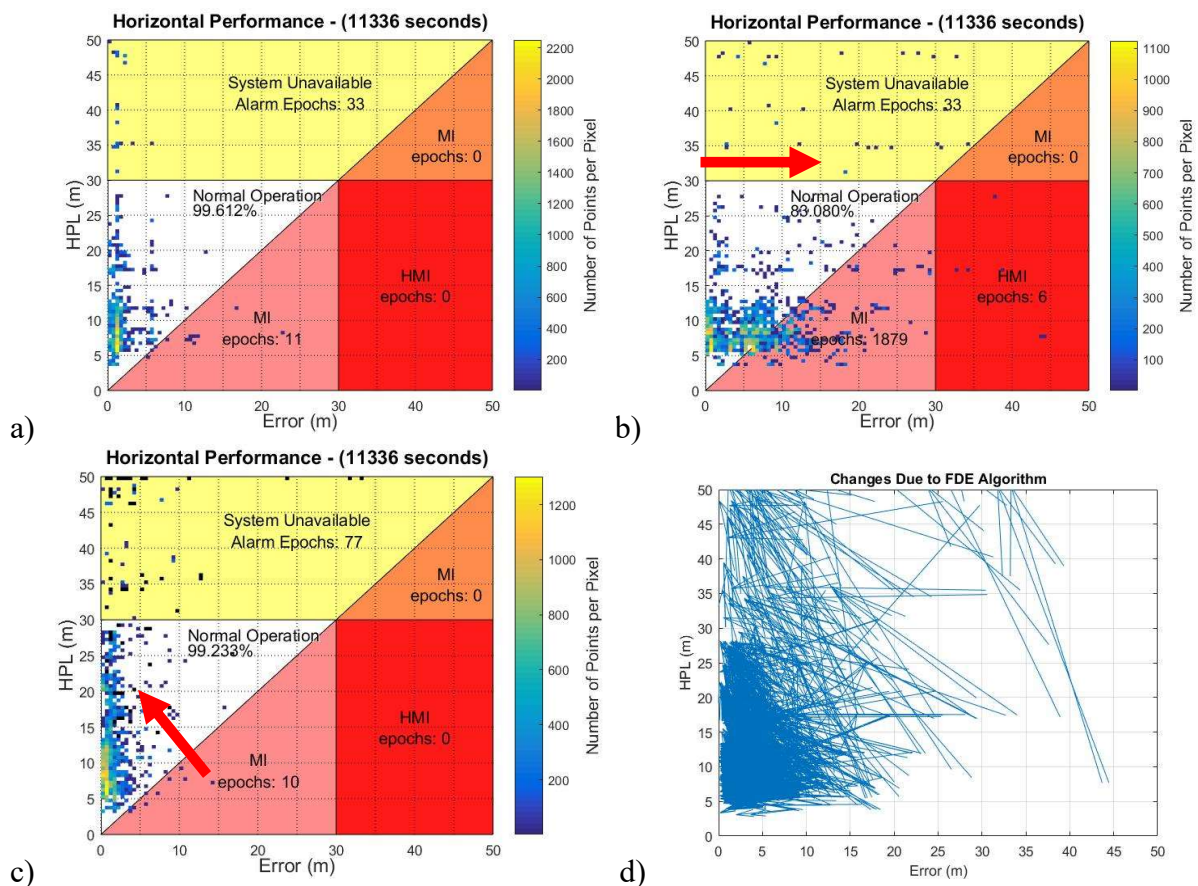


**Figure 6:** Albert Park data a) un-modified data, b) 20m pseudorange error added to 1 random satellite 50% of the time, c) FDE carried out on data with manually added pseudorange error and d) the change in position for each point on the diagram from b to c.

Adding pseudorange error does not affect the HPL calculation however it will affect the position error. This results in the data shifting to the right in a similar manner to the CBD data shown in Figure 5. Conducting FDE however removes the satellites from the solution so the HPL will increase (by how much depends on the satellite geometry) and the HPE will decrease as the faulty pseudoranges are no longer part of the position solution. This results in most of the data moving up and to the left as seen in section c) and d) of Figure 6.

The percentage of normal operation in Figure 6 decreases by 16.5 percentage points once the erroneous pseudoranges were added. Using the FDE algorithm, the normal operation rises to 99.2% which is still less than the clean data but that is to be expected since pseudoranges

have been removed and some points have been pushed into the System Unavailable space. This lower percentage gives a more accurate representation of the integrity of the system.

These plots also show that not all faulty points are moved out of the misleading information zone. This is likely due to the number of iterations of FDE carried out in this test series. If more iterations were completed, more faulty points will be captured and adjusted. However, this comes at a cost of losing satellites for position calculations. Plot c) in the above figures shows that the faulty data will often move towards the System Unavailable section of the diagram depending on its faulty values. This is the desired outcome as in the System Unavailable section, the user is warned that the integrity of the system is such that the position cannot be trusted for that epoch rather than no warning being generated for a hazardous position solution.

### 5.3 Fault Detection and Exclusion

The FDE loop was iterated as many times as necessary to remove the maximum pseudorange error in each faulty epoch for both the Albert Park and Melbourne CBD data whilst maintaining a minimum of 4 satellites for position calculations. No pseudorange errors were added to the data shown in Figure 7. As seen in Figure 6c, not all faulty points were corrected. In the CBD data, a lot of the faulty points shifted to the System Unavailable section of the diagram. The same process occurred in the Albert Park data however it's less obvious due to much fewer erroneous data points.

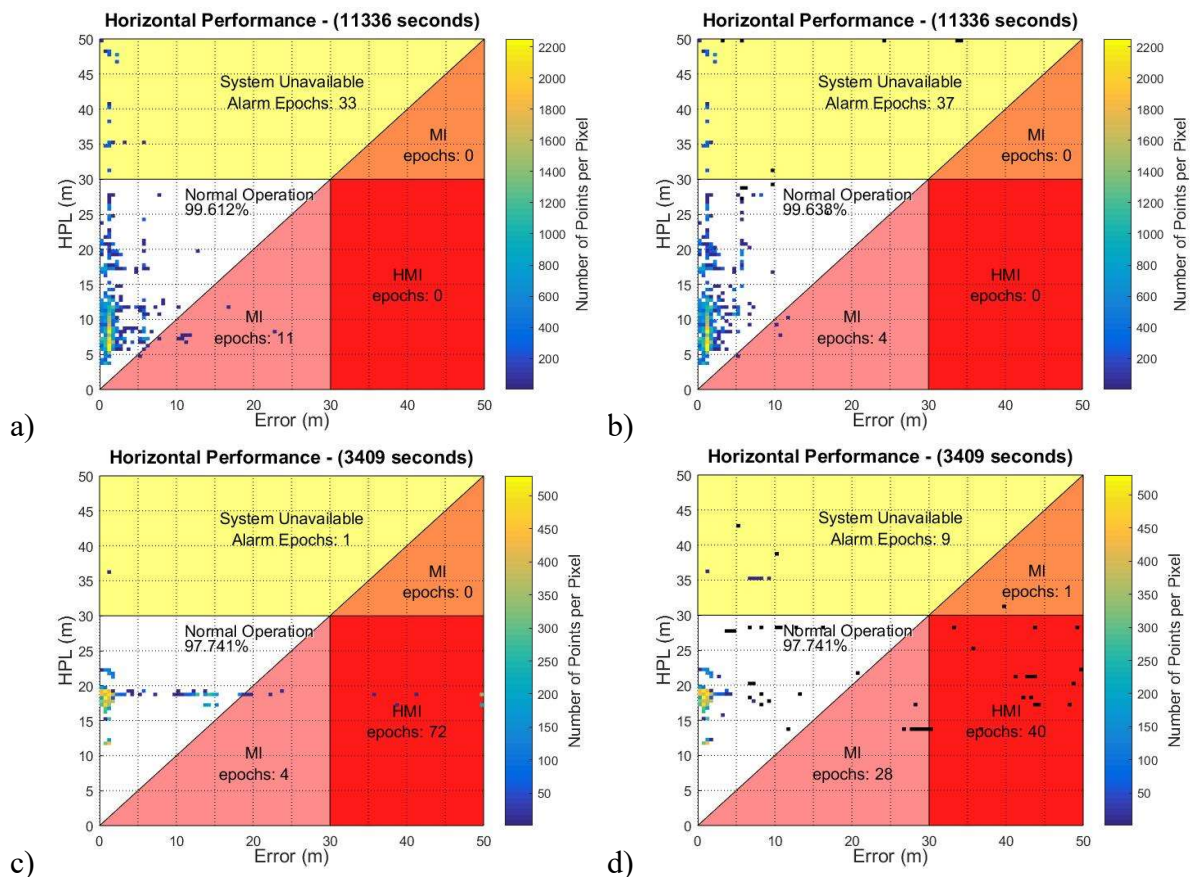


**Figure 7:** Albert Park (a-b) and Melbourne CBD (c-d) data before and after the implementation of FDE algorithms

Figure 7d) shows the data points (black points) that could no longer be processed through the FDE algorithm due to a lack of satellites available. This accounts for all the points below the diagonal line as well as some above. This shows that there is a need for more satellites or more information from other sources to achieve a high quality, high integrity data set.

For each point that was detected as faulty as part of the FDE process, the corresponding pseudorange error was monitored. Figure 8 shows the number of occurrences in each bin of pseudorange errors that were corrected.

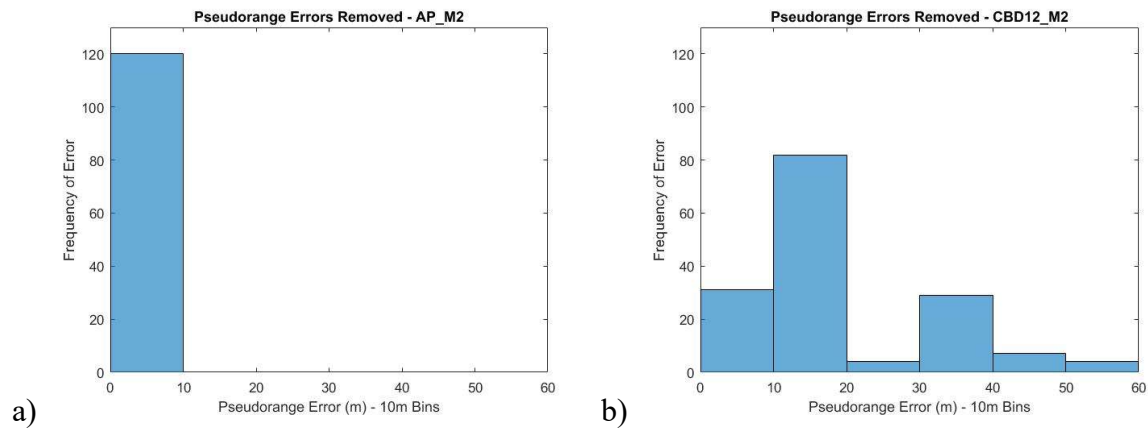


**Figure 8:** The occurrence of pseudorange errors in 10 m bins for each point corrected in the Albert Park data (a) and the Melbourne CBD data (b)

The Albert Park data had approximately 120 erroneous data points however the Melbourne CBD data had over 150 points corrected. The histograms show that all of the pseudorange errors are less than 10 m for Albert Park and less than 60 m for Melbourne CBD. This indicates that in Albert Park there is most often only one reflection occurring before the receiver detects the signal, however in the CBD there are many reflections resulting in a much larger pseudorange error.

To quantify the results displayed above, Figure 9 was created to demonstrate the changes in the data after the faulty pseudoranges had been removed. The pie charts are split up according to sections within the Stanford Integrity Diagram. The sections are labelled: Normal Operation, System Unavailable and HMI/MI which amalgamates the Hazardously Misleading Information (HMI) and Misleading Information (MI) sections.



**Figure 9:** Percentages of data points per section of the Stanford Integrity Diagram

Figure 9 shows the Albert Park pie charts on the top remain largely unchanged after the FDE algorithm is applied due to the small number of pseudoranges changed. The Melbourne CBD pie charts on the bottom of Figure 9 shows a similar story due to the small number of points moving between sections.

For comparison, the Albert Park data with the added pseudorange error was compiled into Figure 10 with the effect of the FDE algorithm easily shown.



**Figure 10:** Percentages of data points per section of the Stanford Integrity Diagram for the Albert Park data with added pseudorange errors before and after FDE

There is an almost complete removal of all HMI/MI data from the set using the FDE process. There is a slight increase in the system unavailable section which is to be expected.

The quantity of data points that are shown in Figure 9 are given in Table 2 below. These tables show quantitatively the effect of the FDE process in terms of the number of points in each section of the Stanford Integrity Diagram.

	AP	AP after FDE	CBD	CBD after FDE
<b>Total Points</b>	11336	11336	3409	3409
<b>Normal Operation</b>	11292	11295	3332	3331
<b>Sys Unavailable</b>	33	37	1	9
<b>HMI</b>	0	0	72	40
<b>MI zone 1</b>	11	4	4	28
<b>MI zone 2</b>	0	0	0	1

**Table 2:** Number of points per section (and percentage of total data set) in the Stanford integrity diagram

For the Albert Park data shown in Table 2, the distribution of points does change after FDE however the number of points is so small, it is not quantified in Figure 9. Table 3 shows the same quantitative perspective for the data shown in Figure 10.

	AP with errors	AP with errors after FDE
<b>Total Points</b>	11336	11336
<b>Normal Operation</b>	9418	11249
<b>Sys Unavailable</b>	33	77
<b>HMI</b>	6	0
<b>MI zone 1</b>	1879	10
<b>MI zone 2</b>	0	0

**Table 3:** Number of points per section (and percentage of total data set) in the Stanford integrity diagram for the data with manually added pseudorange errors

These results show that the FDE methodology used in this research works in the CBD and with simulated multipath. It does not achieve 100% faulty data isolation however this is due to the low number of iterations in the fault detection loop and a low number of visible satellites, limiting removal of pseudoranges.

## 6. CONCLUSION

The FDE algorithm used in this paper does not appear to greatly increase the Normal Operation percentage of the data set which is due to the lack of data points and lack of satellites visible. The benefit of the FDE algorithm is better articulated through the simulated data that shows that when enough satellites are available to remove faulty points, the improvement can be up to 13% in the Normal Operation zone.

The work in this paper shows three things. Firstly, conventional RAIM algorithms don't consider the effects of multipath on position error as reflected by an unchanged HPL when pseudorange errors were manually added. Whilst this is an expected result, it is interesting to show the effect of multipath in the vehicle domain in the RAIM context. An additional FDE algorithm is needed to detect and remove erroneous pseudoranges arising from multipath effects. Secondly, removal of erroneous pseudoranges can improve the operation of a navigation system by both bringing back erroneous position solutions into the normal range and by pushing untrustworthy positions above the alarm limit to generate a warning. Thirdly, GPS alone is not enough to provide a high integrity position solution as highlighted by the



number of points not affected by the FDE algorithm due to lack of satellites. More satellites will improve the integrity and availability of the data.

The analysis in this paper uses post processing with highly accurate truth data. To apply it to a real time scenario, it will need to be adapted to take estimates from a prediction algorithm such as a Kalman Filter and compare with measured position solutions. A further step towards implementation would be to fuse in other sensor data such as Inertial Navigation Systems (INS) or Dedicated Short Range Communication (DSRC) outputs.

## 7. REFERENCES

Blanch J, Walter T, Enge P. (2013). Advanced RAIM System Architecture with a Long Latency Integrity Support Message. In: 26th International Technical Meeting of the ION Satellite Division, ION GNSS+, Nashville, Tennessee, pp. 2605-2613.

Brown RG. (1992). A Baseline GPS RAIM Scheme and a Note on the Equivalence of Three RAIM Methods. *Navigation*, 39, 301-316. doi: 10.1002/j.2161-4296.1992.tb02278.x.

Bruckner D. (2014). Protection Level Toolbox. In: Mathworks File Exchange. Mathworks.

Bruckner DC. (2010). On the treatment of noise and conspiring bias in dual-frequency differential global navigation satellite systems. Ohio University.

Hansen AJ. (1997). WAAS Precision Approach Metrics. Accuracy, Integrity, Continuity and Availability. In. WADGPS Laboratory - Stanford University.

Hewitson S, Wang J. (2010). Extended Receiver Autonomous Integrity Monitoring (eRAIM) for GNSS/INS Integration. *Journal of Surveying Engineering*, 136, 13-22.

ICAO. (2001). Annex 10—Aeronautical Telecommunications. Volume II: Communication Procedures.

Jiang Z, Groves PD, Ochieng WY, Feng S, Milner CD, Mattos PG. (2011). Multi-constellation GNSS multipath mitigation using consistency checking. In: Proceedings of the 24th International Technical Meeting of The Satellite Division of the Institute of Navigation (ION GNSS 2011). Institute of Navigation, pp. 3889-3902.

Ochieng WY, Sauer K. (2002). Urban road transport navigation: performance of the global positioning system after selective availability. *Transportation Research Part C: Emerging Technologies*, 10, 171-187. doi: [http://dx.doi.org/10.1016/S0968-090X\(02\)00008-6](http://dx.doi.org/10.1016/S0968-090X(02)00008-6).

Takasu T. (2011). RTKLIB: An open source program package for GNSS positioning. In.

Tossaint M, Samson J, Toran F, VENTURA-TRAVERSE J, HERNANDEZ-PAJARES M, Juan J, Sanz J, RAMOS-BOSCH P. (2007). The Stanford–ESA Integrity Diagram: A New Tool for The User Domain SBAS Integrity Assessment. *Navigation*, 54, 153-162.